AIP | Journal of Applied Physics

Faster radial strain relaxation in InAs–GaAs core–shell heterowires

Karen L. Kavanagh, Igor Saveliev, Marina Blumin, Greg Swadener, and Harry E. Ruda

Citation: J. Appl. Phys. **111**, 044301 (2012); doi: 10.1063/1.3684964
View online: http://dx.doi.org/10.1063/1.3684964
View Table of Contents: http://jap.aip.org/resource/1/JAPIAU/v111/i4
Published by the American Institute of Physics.

Faster radial strain relaxation in InAs–GaAs core–shell heterowires

Karen L. Kavanagh,[1,a)] Igor Saveliev,[2] Marina Blumin,[2] Greg Swadener,[3] and Harry E. Ruda[2]
[1]*Department of Physics, Simon Fraser University, Burnaby, British Columbia V5A 1S6, Canada*
[2]*Centre for Advanced Nanotechnology, University of Toronto, 170 College Street, Toronto, Ontario M5S 3E4, Canada*
[3]*Mechanical Engineering and Design, Aston University, Aston Triangle, Birmingham B4 7ET, United Kingdom*

(Received 27 September 2011; accepted 12 January 2012; published online 17 February 2012)

The structure of wurtzite and zinc blende InAs–GaAs (001) core–shell nanowires grown by molecular beam epitaxy on GaAs (001) substrates has been investigated by transmission electron microscopy. Heterowires with InAs core radii exceeding 11 nm, strain relax through the generation of misfit dislocations, given a GaAs shell thickness greater than 2.5 nm. Strain relaxation is larger in radial directions than axial, particularly for shell thicknesses greater than 5.0 nm, consistent with molecular statics calculations that predict a large shear stress concentration at each interface corner. © *2012 American Institute of Physics*. [doi:10.1063/1.3684964]

I. INTRODUCTION

In planar epitaxial growth, a thin film with lattice constant, a_f, grown on a thick, single crystalline and large area substrate, lattice constant, a_s, deforms tetragonally in response to interfacial strain from lattice mismatch, $f = \Delta a/a_s$. As the film is much thinner than the substrate, the majority of this strain is elastically accommodated by the film. With increasing film thickness, volume strain energy accumulates until surface roughening,[1] islands,[2] and/or dislocations[3] begin to reduce this energy to relax the strain. The equilibrium critical thickness for dislocation formation is defined as the thickness when the volume strain energy equals the energy of an interfacial, edge dislocation, or misfit dislocation.[3] In free-standing, heterostructural nanowires, either axial or core–shell, the radial dimensions are finite, but size is effectively infinite along the wire growth direction. Such three-dimensional geometries dramatically modify the theoretical critical thresholds for strain relaxation.[4–9] For nanowire core diameters below critical thresholds, the volume strain energy is too small for dislocations, meaning coherent axial or core–shell geometries are theoretically feasibly consistent with experimental observations.[10] Barriers to the nucleation of misfit dislocations have often resulted in larger critical thicknesses in planar systems,[11] also likely true for nanowires.

There are very few experimental reports of strain-relaxation in axial or core–shell nanowires. Two examples, both systems grown via metalorganic chemical vapor deposition (MOCVD), include partial relaxation of an axial gallium-arsenide (GaAs) on indium-arsenide (InAs) (111)B wire (20 nm radius) (5 nm GaAs shell layer) based on dark field transmission electron microscopy (TEM) analysis,[12] and core–shell (silicon)–(silicon–germanium) nanowires where partial axial relaxation due to surface roughening and dislocation formation was reported.[13] Strain relaxation in the core–shell Ge(111)–Si system is also being investigated.[14] Strain relaxation in the wurtzite (WZ) InAs–GaAs core–shell system has been reported by at least two other groups.[15,16]

In a previous paper, we described the structure and defects from strain relaxation in the core–shell, InAs–GaAs nanowire system grown by molecular beam epitaxy (MBE).[17] Wurtzite phase heterowires with preferred growth directions (001) and hexagonal sidewall facets were investigated. The radii of the InAs cores (11–26 nm) all exceeded theoretical critical core radii values (>2 nm)[8] with GaAs shell thicknesses greater than 2.5 nm. Strain relaxation via dislocations was observed with the degree of radial relaxation in most cases, greater than axial strain relaxation. Interestingly, in those wires with the smallest shell thicknesses (2.5–5.0 nm) only axial relaxation was detected. Calculations conflict as to which direction should relax first.[4,7,8] The percentage axial strain relaxation of the WZ wires increased exponentially with shell thickness (normalized to the core size) more slowly than radial strain relaxation, which was comparably more abrupt. Extrapolation indicated a critical shell-to-core ratio for axial strain relaxation at these core radii of 0.1. Correlated with the strain relaxation, electrical measurements of field-effect transistors fabricated from these strain-relaxed nanowires demonstrated a suppressed field-effect-mobility as compared with bare InAs nanowires, that was independent of InAs core diameter.

In this paper we expand our discussion of the WZ heterowires and compare them to zinc blende (ZB) heterowires that grew simultaneously with (001) growth orientations. The bulk ZB lattice constants of GaAs and InAs ($a_{GaAs} = 5.6533$ Å; $a_{InAs} = 6.0583$ Å)[18] give a ZB mismatch with respect to the average lattice constant, $f_{ZB} = \Delta a/a_{average} = 6.92\%$. The WZ phases of these semiconductors are commonly encountered in nanowires grown via vapor-liquid-solid processes,[15,16] but the equilibrium lattice constants are less well known than the thermodynamically more stable ZB phases. Bulk WZ InAs[19] and GaAs[20] crystals can only be formed at high pressures and temperatures, but are both stable when cooled to room temperature

a)Author to whom correspondence should be addressed. Electronic mail: kavanagh@sfu.ca.

TABLE I. Summary of the MBE growth details for the InAs–GaAs core–shell nanowires of this study, including sample number, No., Growth temperature, T, Effective planar thickness, d, Growth rate, d/t, and Radii thickness, s. Average wire lengths were 0.1–1 μm (ZB) and up to 5 μm (WZ).

No.	Core shell	T (°C)	d (nm)	d/t (nm/min)	s (nm)
1	InAs	400	130	3.3	10–60
	GaAs	400	20	5	3–15
2	InAs	400	130	3.0	10–60
	GaAs	400	40	4	3–30
3	InAs	400	43	1.7	10–60
	GaAs	480	80	4	10–60

and atmospheric pressure. They have larger c-axis (0002) planar spacings (WZ GaAs: a = 3.989 Å, c = 6.564 Å; WZ InAs: a = 4.27 Å, c = 7.02 Å) compared to the corresponding bulk ZB (111) spacing but nevertheless, a slightly *smaller* lattice mismatch, $f_{WZ} = \Delta a/a_{average}$= 6.80% (WZ) compared to ZB.

In ZB (001) heterowires the growth cross-section is square or rectangular with four sidewall {110} interfaces. Such interfaces are rarely studied in planar heteroepitaxial systems,[21] but encountered in heterowires presumably as their non-polar character provides the most stable surface facets. Similar to the WZ heterowires, strain relaxation occurs faster in radial directions than along the axial growth direction.

II. EXPERIMENT

InAs (core)-GaAs (shell) heterowires were grown using MBE (solid sources) using GaAs (001) oriented substrates. Once inside the growth chamber, the substrates were baked at 590 °C for 30 min. An undoped GaAs buffer layer was grown at a temperature of 480 °C. Gold films of 0.5 nm average thickness were deposited *in situ* in the growth chamber at 580 °C and subsequently annealed for 5 min at the same temperature. An initial exposure to Ga and As beams was carried out at a temperature of 480 °C prior to a change to In and As fluxes at a lower temperature, 400 °C. Subsequent GaAs layers were grown at 400 or 480 °C. The substrates were not rotated. A summary of growth details for wires investigated in this paper are shown in Table I. Based on field-emission secondary electron microscopy (SEM) studies of the Au deposition and resulting InAs wires grown in a similar manner, but without the GaAs shell, the radii of InAs wires—equal to the radii of Au islands on top of the wire—varied from 10 to 60 nm.

Samples of nanowires were prepared for TEM by transfer onto carbon-coated Cu grids. Transfer was accomplished either by ultra-sonic removal in ethanol solutions followed by evaporation of pipette drops or simply by touching the grid with the surface of the MBE samples. Plan-view or cross-sectional images of the wires were obtained by embedding the wires in epoxy followed by standard mechanical polishing and Ar-ion milling. The electron microscopy was carried out at an operating voltage of 200 keV (0.23 nm point-to-point resolution) with a microscope equipped with either a field-emission gun or LaB_6 thermal electron source. Scanning TEM including energy dispersive spectroscopy (EDS) was carried out with the former source.

III. RESULTS

Figure 1 shows secondary electron SEM images obtained with the electron beam perpendicular to the sample surfaces (zero sample tilt). The edge of each image is aligned with the ⟨110⟩ cleaved wafer edges. The low magnification image of sample 1 in Fig. 1(a) and higher magnification image of sample 2 in Fig. 1(b) show a dense, forest of nanowires ranging in length from 0.1 to 3 μm or more, with maximum shell thicknesses of 15 and 30 nm, respectively. Some of the wires (circled in each image) have grown within 5° of being (001) oriented, whereas most are tilted away from the normal, some with large radii of curvature. The wires shown in Fig. 1(b) are ZB with a square or rectangular cross-section with sidewall lengths that range between 20 and 100 nm. They have stepped sidewall facets aligned parallel or at an angle of 45° to the cleaved ⟨110⟩ wafer edges. The end of these ZB wires invariably shows a kink in growth direction abruptly toward a particular ⟨111⟩ direction most likely (111)B.[22] There are shorter, narrower wires aligned with the ⟨110⟩ wafer edges that are growing completely in a ⟨111⟩ direction.

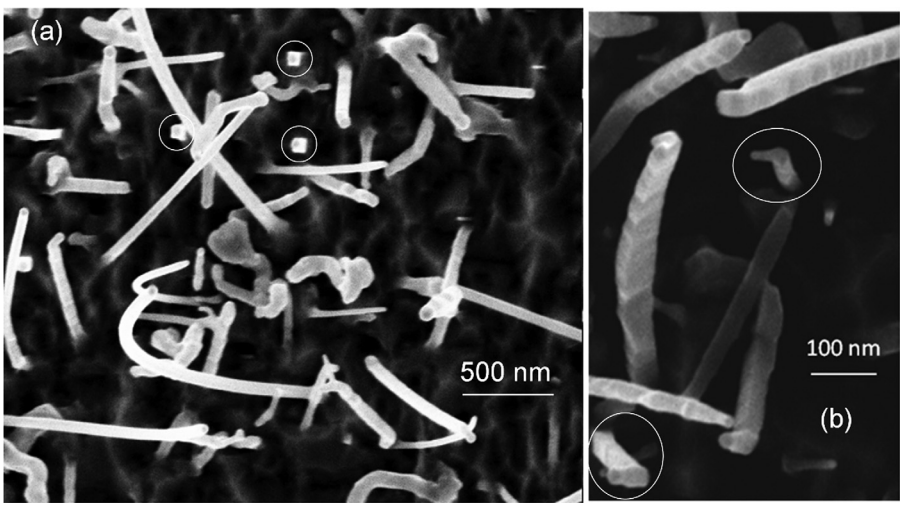

FIG. 1. Secondary electron micrographs of (a) sample 1 and (b) sample 2 viewed perpendicular to the surface (sample tilt zero). The edge of each image is aligned with the ⟨110⟩ wafer edge. The circled wires are ZB nanowires (square cross-section) that have grown closest to perpendicular (001).

Cross-sectional TEM investigations of nanowires transferred to a grid, found both ZB and WZ heterowires. The WZ wires tended to be longer with smoother, hexagonal sidewalls, with smaller core radii compared to the ZB, but shell thicknesses were of comparable range. An example of a WZ nanowire imaged from the side is shown in Fig. 2. The selected area diffraction (SAD) pattern indicates a $\{1\underline{2}10\}$ orientation with a growth direction [0001]. The radial directions and side facets in this orientation are therefore $\langle 10\underline{1}0\rangle$. Nanowires tilted close to any strong diffraction condition always showed fringes within the core region that ended at the sidewall interfaces. In this case the tilt is such that the (0002) planes have the strongest diffraction intensity giving Moiré fringes (period 8 nm) parallel to the growth direction. These delineate a core (radius 27 nm) with an asymmetric shell thickness, in this case, 5 nm on one side and 10 nm on the other. The Moiré pattern varies from the center outward due to the surface slope and variations in the thickness of the core and shell layers. There is also the possibility that the interfaces are $\{1\underline{2}10\}$ type rotated 30° to the surface $\{10\underline{1}0\}$.[16] If the wires were coherently strained then there would be only one spot pattern associated with an average strained lattice constant that depends on the ratio of core to shell volumes. The InAs core would be in compression, whereas the shell in tension. As multiple spots were visible in this wire, and in all wires investigated, strain relaxation has occurred.

In those WZ wires where both sidewall thicknesses were less than 5 nm, radial strain relaxation was not detected. Figure 3 shows one example. The lower magnification image shows the wire with Moiré fringes again within the core region with thinner shell thicknesses. The higher magnification image shows the thicker left sidewall, which has an average shell thickness 4.2 nm. The SAD again shows multiple spots but only along the [0001] growth direction. In the radial direction spots are elongated, consistent with the smaller length scale, but are not separated, nor rotated. Radial strain relaxation has not yet occurred.

Figure 4 shows a low magnification, bright field (BF) TEM image from a typical ZB (001) nanowire imaged in side view (110). A clear core–shell nanostructure is visible with a change in growth direction and phase apparent near the Au particle. The InAs core radius tapers from the bottom to top (from 27 to 14 nm), whereas the GaAs shell thickness is asymmetric but relatively uniform, in this case, 30 nm on the left and 10 nm on the right. The widely spaced contrast visible perpendicular to the growth direction is due to sample bending indicating that the wire is curved out of the plane of the image consistent with wires observed in the SEM. The higher magnification image of the lower part of the wire shows strong fringes (average spacing 5.3 nm) within the

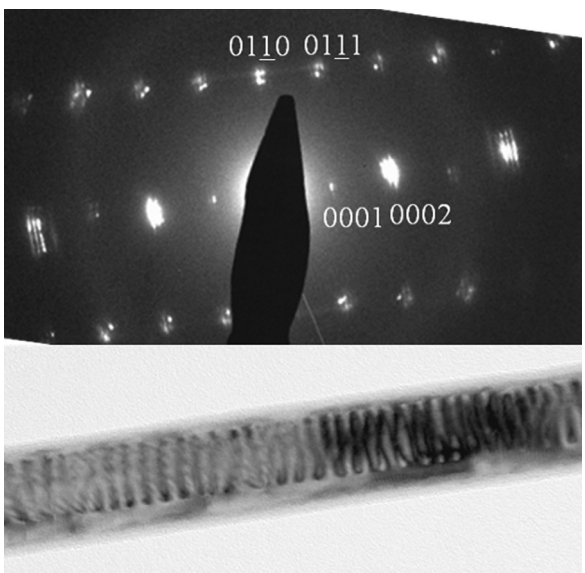

FIG. 2. Bright field TEM image and selected area diffraction pattern $(11\underline{2}0)$ of a WZ wire showing relaxation. Multiple spots associated with any particular (*hkil*) is explained by double diffraction.

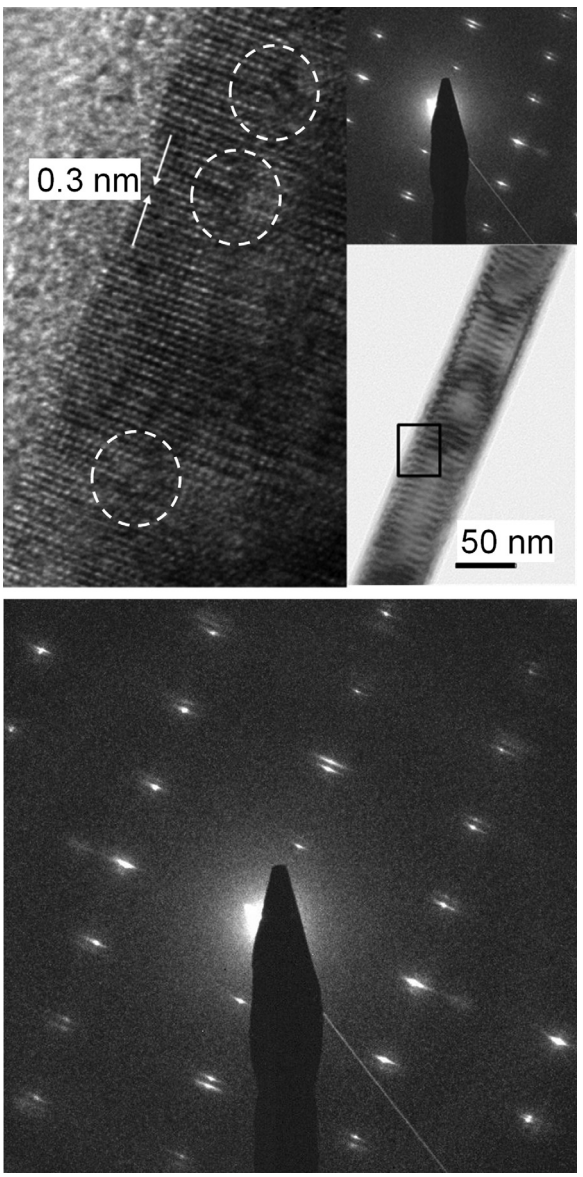

FIG. 3. Lattice image of a WZ wire (60 nm diameter; left shell thickness 5 nm) showing dislocations (circled) at the shell-core interface. The insets show a lower magnification bright field image of the heterowire with its corresponding selected area diffraction pattern magnified below indicating a $(11\underline{2}0)$ image plane. Radial relaxation has not occurred in this wire. Axial relaxation is 4.7% with an average dislocation spacing of 7.2 nm.

core region aligned with the direction of local sample tilt. There are also parallel defects visible, aligned with a ⟨121⟩ direction, which often pass through the core and one or both shells. EDS analysis profiling (not shown) confirmed that the In composition is highest within the middle region, whereas that of Ga, in the shell. Although the core–shell region is ZB, WZ [0001] GaAs growth has extended the end at the Au particle.

The degree of strain relaxation of individual wires, R, as a percentage of the maximum mismatch was measured parallel and perpendicular to the growth direction using each SAD pattern. Complete relaxation would mean that at a given (hkl) or ($hkil$) spot the spacing between that of the inner spot (InAs) compared to the outer spot (GaAs) normalized to their average value would be equal to the lattice mismatch (0.069). Values less than that would indicate partial relaxation. Results for R from ZB wires versus the ratio of shell thickness to core radius, are plotted in Fig. 5. The solid lines are least square linear fits. Similar data from WZ wires was reported previously.[17] In both cases radial strain relaxation (in the plane of each TEM image) was more rapid than in the axial direction parallel to the long direction. Over the range of ZB wire geometries investigated (shell thickness-to-core radius 0.5–1.7) the radial strain relaxation was 95 ± 5% independent of wire size, whereas axial strain relaxation increased from 70% to 95%. Unlike WZ wires, no wires were found with zero radial relaxation but one GaAs shell thickness was always greater than 9 nm.

The percentage strain relaxation can also be estimated from the Moiré fringe spacings, D_{hkl}, for a particular diffraction condition. Translational Moiré fringes decrease in spacing with relaxation to a minimum spacing, D^m_{hkl}, at $R = 100\%$ given simply by

$$D^m = \frac{1}{g_{\mathrm{InAs}} - g_{\mathrm{GaAs}}} = \frac{d_{\mathrm{GaAs}} d_{\mathrm{InAs}}}{d_{\mathrm{InAs}} - d_{\mathrm{GaAs}}}$$

where g is the reciprocal space diffraction spot position for a particular (hkl). For partial relaxation $R = D_{\mathrm{min}}/D$. Assuming bulk lattice constants the minimum spacing, $D^m_{004} = 2.1$ nm (ZB), $D^m_{220} = 3.0$ nm (ZB), or $D^m_{0002} = 5.0$ nm (WZ). Consistent with the data from diffraction, the axial relaxation based on Moiré fringes ranged from 40 to 95 ± 5% and was always less than the corresponding radial value which was near 100%.

We are expecting to find dislocations in these wires to explain the strain relaxation observed. Dislocations are already visible in the WZ and ZB wires shown in Figs. 3 and 4. The circled regions in Fig. 3 indicate edge dislocations located at the sidewall WZ $\{10\bar{1}0\}$ interfaces, Burger's vector $\mathbf{b} = (c/2)[0001]$ with line directions $\mathbf{u} = \langle 12\bar{1}0 \rangle$ into the page. This type of dislocation is relaxing axial strain at a rate of $\delta = |\mathbf{b}|/D_e$, where D_e is their linear spacing. In this wire the average spacing was 7 nm so $\delta = 0.047$ equal to the relaxation indicated by the diffraction spot spacing.

In the ZB wires there were clearly visible defects running along one set of {111} planes across the core and often into the shells. Figure 6 shows a pair of BF images from the same region of another nanowire, comparing diffraction contrast from {220} and {111}. Diffraction normal to the defects causes a total loss of their contrast. Moiré fringes are visible as before, but the line defects are no longer visible. Figure 7 shows a pair of dark field (DF) TEM images from another ZB wire tilted (a) parallel and (b) perpendicular to

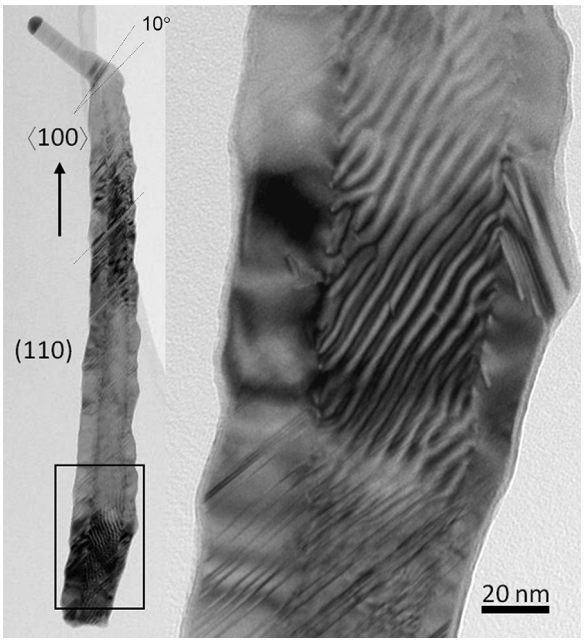

FIG. 4. Bright-field TEM image of a ZB InAs–GaAs (001) core–shell nanowire. The image plane is (110). The InAs core radius tapers from bottom to top (from 27 to 14 nm), whereas the average shell thickness is asymmetric, 10 nm at the right and 30 nm on the left side, but remains relatively constant.

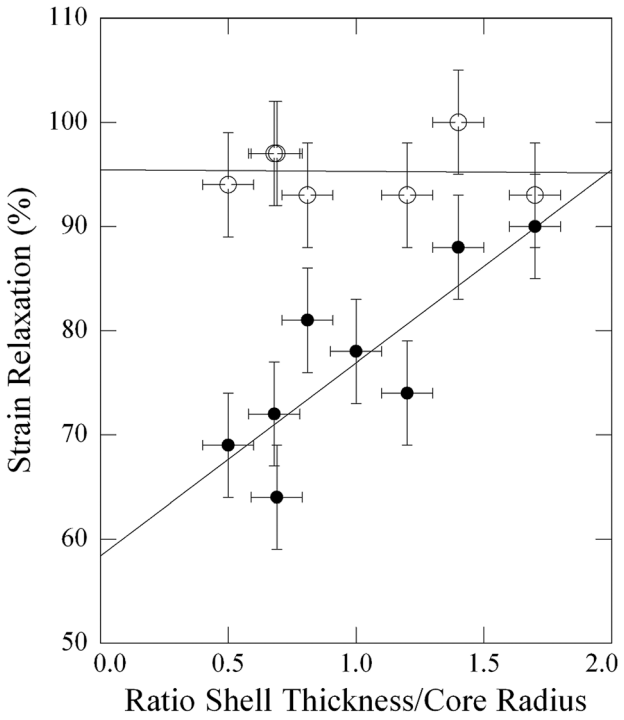

FIG. 5. Plot of percentage strain relaxation vs the ratio of the shell thickness to core radius for individual ZB heterowires in radial (○) and axial (●) wire directions.

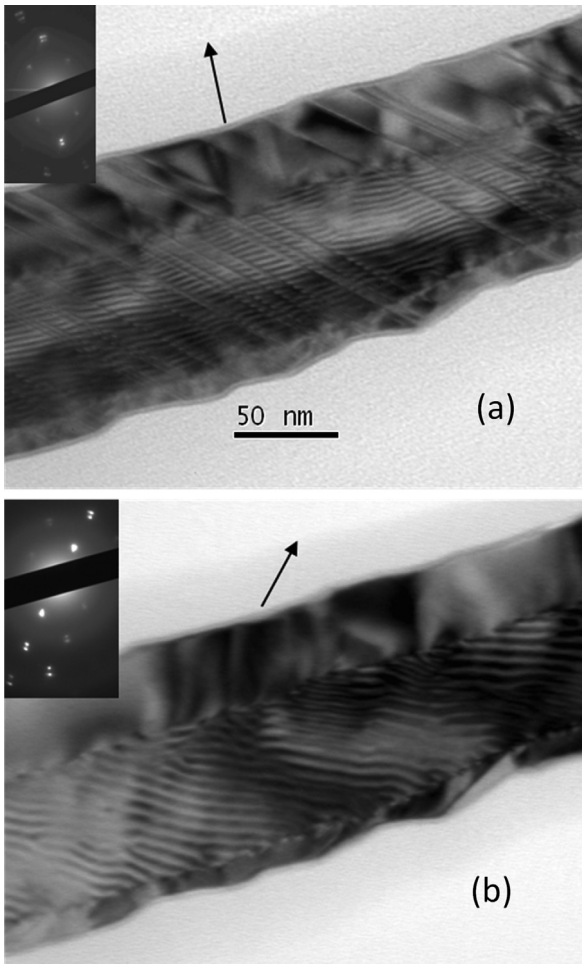

FIG. 6. Dark-field TEM images of the same area of a ZB wire tilted toward (a) {220} and (b) {111} diffraction planes. The arrows point in the direction of the diffraction vector (normal to the diffracting planes in each case).

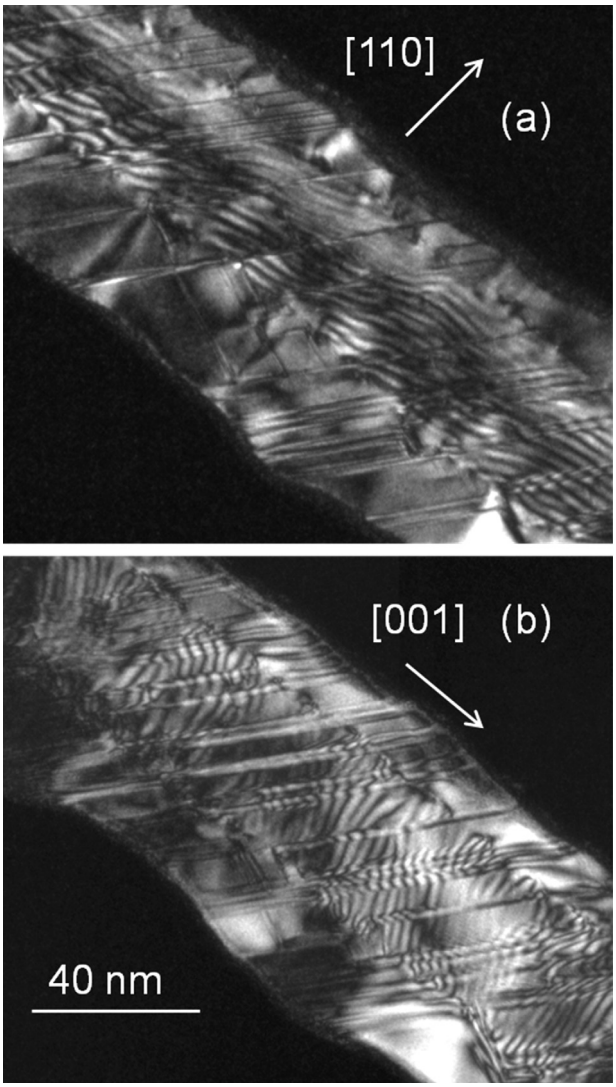

FIG. 7. Dark field TEM images of the same area of another ZB wire tilted about axes parallel and perpendicular to the wire length toward (a) {220} and (b){004} diffraction planes. The arrows point in the direction of the diffraction vector (normal to the diffracting planes in each case).

its length. Strong {220} and {004} diffraction conditions were obtained, respectively. Moiré fringes are visible perpendicular to the diffraction vector in both cases, within the middle region where the top and bottom GaAs shells overlap the InAs core. Notice that the {220} Moiré fringes pass through the defects relatively unchanged, whereas those from {400} change direction to run parallel [001] The line-type contrast parallel to a $\langle 121 \rangle$ direction remains visible in both tilted orientations. Any deviation from parallel fringes is due to local variations in strain relaxation and/or a relative twist in the two lattices. All of this evidence points to these defects being {111} stacking faults due to the glide of a $\mathbf{b} = (a/6)\ \langle 121 \rangle$ partial dislocation on these planes. Such dislocations are screw-type and hence do not relax mismatch strain but would generate a twist in the shell with respect to the core. Given their linear density, D, on average 4 nm, they would contribute a twist in the shell of $\theta = |b|D = 5^\circ$. Further support is clear from the 10° angle of the {0002} stacking faults, visible in the WZ GaAs extension at the Au particle in Fig. 4, with respect to these defects in the ZB shell. The WZ GaAs extension of the core would have occurred during the initial formation of the shell. Its (0002) planes would therefore, be parallel to the core (111) planes. The shell has rotated clockwise due to the dislocations that have formed in the shell, in response to the curvature stress introduced by the asymmetric shell growth rates. These dislocations would have nucleated first on the thicker shell side with the polarity necessary to rotate clockwise to relax elastic strain.

Stacking faults and misfit dislocations relaxing axial strain are also visible in higher magnification images of the ZB heterowire sidewall interfaces. Figure 8 shows an image of a sidewall region from one of the ZB wires. The {111} stacking faults described previously are visible in this lattice image running from the shell into the core along one $\langle 112 \rangle$ direction. The circled area has two dislocations each with $\mathbf{b}$ parallel to a $\langle 112 \rangle$ direction, and line directions $\mathbf{u} = \langle 110 \rangle$ (into the page). They are perfect $(a/2)\langle 110 \rangle$ dislocations rather than partial dislocations, as there are no stacking faults associated with them. They have an edge component $\mathbf{b}_e = (a/2)\sqrt{3}/2\langle 110 \rangle$ with a screw component out of the plane of the image not visible here. They add to form a pure edge dislocation $\mathbf{b} = (a/2)[001]$ that relaxes axial strain. For 100% relaxation of the axial mismatch

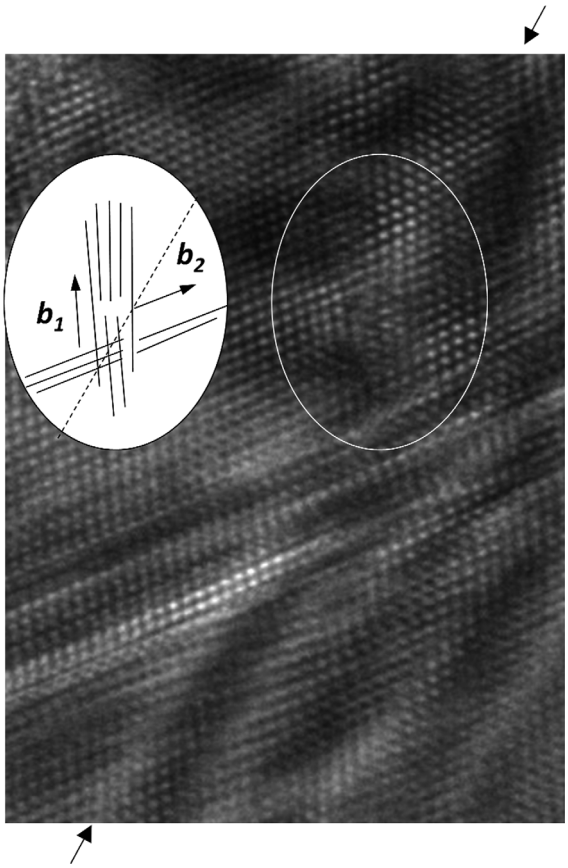

FIG. 8. High-magnification lattice image of a sidewall region of a ZB nanowire. The two arrows indicate the position of a (110) sidewall interface. The circled area identifies the location of two misfit dislocations diagrammed to the left. The line defects running parallel to {111} planes are multiple {111} stacking faults.

strain the linear dislocation spacing, D, would need to be $|\mathbf{b}|/f = 0.28$ nm/$0.069 = 4.1$ nm. Their $D = 6$ nm relaxes strain $(|b|/D) = 0.047$ or R = 67% sufficient to explain the partial axial relaxation detected from diffraction spot analyses.

Stacking faults and dislocations that counteract bending stress were also observed in the WZ wires. Figure 9 shows DF TEM images (a) (0002) and (b) $(10\underline{1}0)$ showing defects with an average period of 9 nm in the left sidewall interface. The defects consist of dislocations, $\mathbf{b} = (-c/2)[0001]$, with $\mathbf{u}$ into the plane of the image at the interface. They are associated with an extra plane in the InAs core side visible in the magnified region from (a) and a ZB stacking fault in the shell visible in the magnified region from (b). These defects are adding mismatch strain into the interface but in doing so are relaxing bending stress from the opposite thicker shell. The thicker shell would initially cause concave bending of the thinner side.

Radial strain relaxation in either the WZ or ZB wires requires interfacial dislocations with an edge component perpendicular to the growth. The simplest case would be pure edge $(a/2)\langle 110\rangle$ for ZB or $(a/6)\langle 2\underline{1}10\rangle$ for WZ heterowires with line directions parallel to the growth. Considering the large degree of radial relaxation a spacing of D = 2.8 nm (ZB) is needed. Attempts to image this fine array using weak

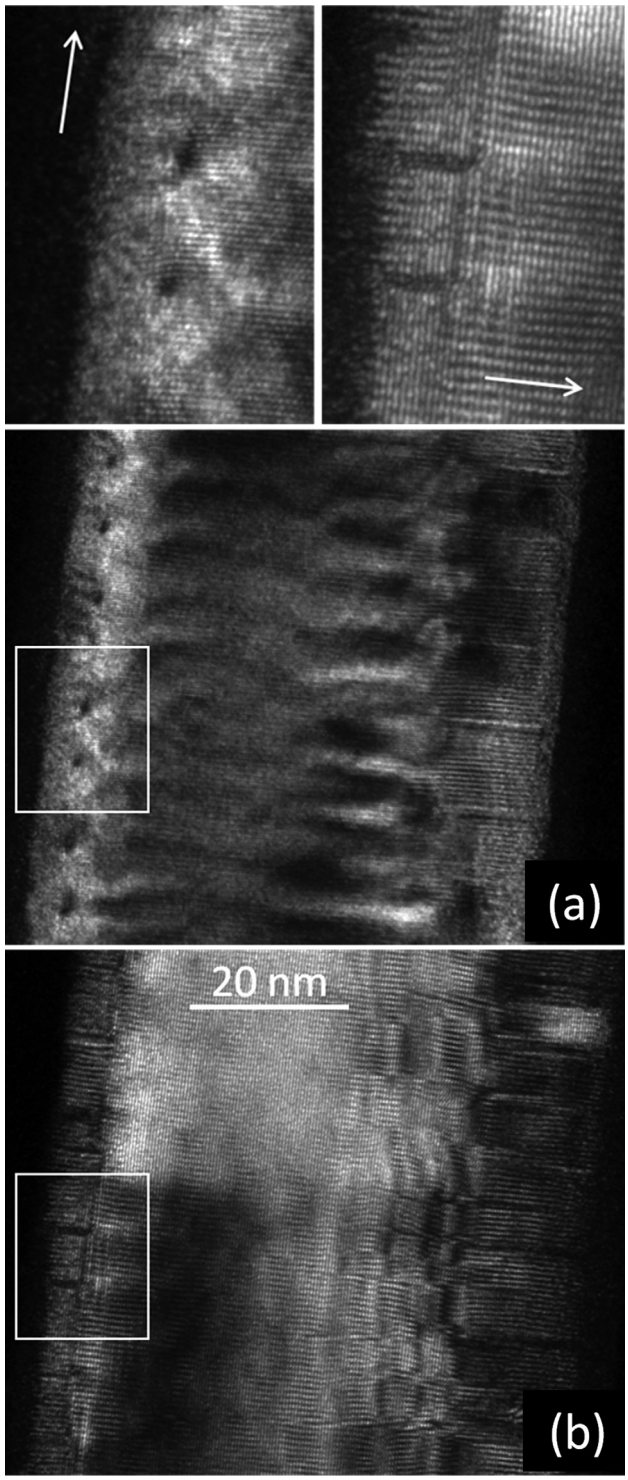

FIG. 9. Dark-field TEM images of a WZ heterowire showing (a) (0002) and (b) $(10\underline{1}0)$ tilt orientations from the same region. Two dislocations and associated stacking faults are highlighted in the magnified images.

beam techniques were unsuccessful. Dislocation contrast was visible when wires were viewed parallel to their growth direction [001] as shown in Fig. 10(a) for the case of a ZB wire. The InAs core has a square shape (side facet length 38 nm) with one side of the shell thinner than 3 nm. The facets are {110} and there is clearly relaxation on three sides of the wire based on the Moiré fringes and dislocation contrast visible. Radial relaxation of 85% was calculated from the

(220) diffraction spot spacing of the SAD pattern in Fig. 10(b). A STEM image with EDS maps of the elemental composition of a similar wire shown in Fig. 10(c), confirms the abruptness of the two binary alloys.

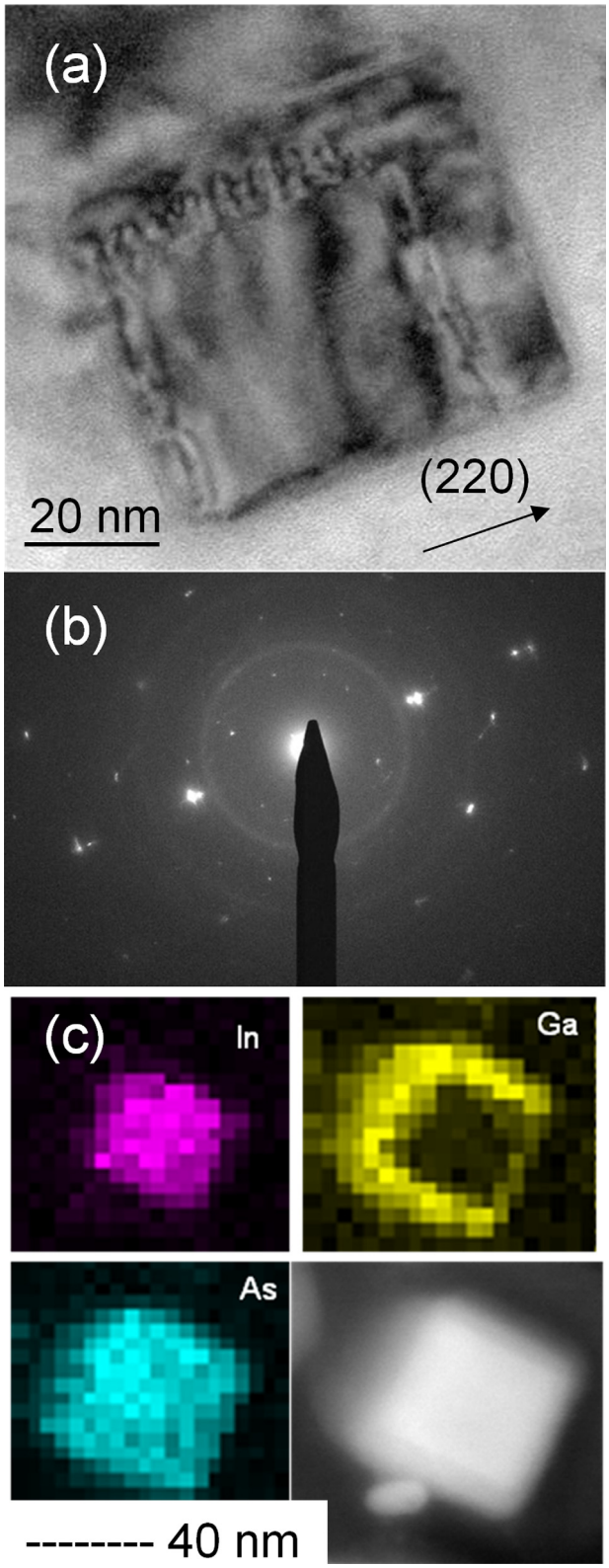

FIG. 10. (Color online) (a) Bright-field TEM image and (b) selected area diffraction pattern of a ZB InAs–GaAs, core–shell heterowire viewed close to its [001] growth direction. Three interfaces are visibly relaxed due to dislocations. (c) Scanning TEM image and energy dispersive x-ray spectroscopy elemental maps of a similar heterowire.

IV. DISCUSSION

Strain relaxation by dislocations was detected in all ZB or WZ oriented InAs/GaAs core–shell heterostructures investigated. The wires had core radii greater than 12 nm, which is greater than the critical radii (2 nm) predicted for this system, where coherently strained heterowires with infinite shell thicknesses would be feasible. For core radii 12 nm or more, relaxation is expected for shell thicknesses greater than ~ 2 nm, only slightly larger than the critical thickness for planar growth (0.6 nm).[23] Based on the analysis of diffraction patterns and Moiré fringes radial strain relaxation detected in both ZB and WZ nanowires, reached $95 \pm 5\%$, and was independent of the shell thickness for shell thicknesses larger than 5 nm. Meanwhile, axial strain relaxation increased more slowly with increasing shell to core ratio. Up to 35% residual axial strain remained in the thinner shell wires. In nanowires with intermediate shell thicknesses between 2 and 5 nm, only axial strain relaxation was detected suggesting that radial relaxation requires a greater shell thickness.

The long curvature of many of the wires visible in SEM and TEM images was no doubt the result of a greater residual tensile strain on the thinner shell side. Stacking faults that formed would counteract such bending stress and were observed in both ZB and WZ wires. Additional rotation of the GaAs shell lattice with respect to the core was evident from misalignments in {111} planes between the core and shell in ZB wires and the opposite polarity shell dislocations and stacking faults in WZ wires. As the surface diffusion length of Ga and In atoms is known to be many microns under these growth conditions, a shadowing of the As flux is most likely causing the asymmetric growth. Radially uniform growth rates are feasibly by MBE by increasing the distance between the Au particles.[16]

Axial strain relaxation of the wires was apparent from edge dislocations visible in the sidewall interfaces of both WZ and ZB wires. In the ZB wires, the dislocations were the common $\mathbf{b} = (a/2)\langle 110 \rangle$, which can form by surface loop nucleation followed by glide on {111} planes intersecting the strained interface. Figure 11(a) shows a drawing of the ZB nanowires with {111} glide planes (shaded) indicated and proposed dislocation nucleation processes. The glide planes that cross the core region are perpendicular to the top interface so dislocations that glide on these planes cannot relieve strain. The same dislocation that nucleates as a loop at the corner (thicker dotted lines) and glides to the interfaces, cause tilt and twist on the top interface, but will result in axial strain relaxation on the side interfaces. Two such dislocations with opposite **b** add to form a pure edge dislocation on the sides that efficiently relieves axial mismatch. These can also split into partial dislocations $\mathbf{b} = (a/6)\langle 112 \rangle$, which were likely responsible for the ZB stacking faults observed on one facet. The situation in WZ nanowires is shown in Fig. 11(b). In this case, the easiest glide processes occur on $\{10\underline{1}0\}$ planes[4] with $\mathbf{b} = (c/2)[0001]$, but there are no available surfaces for such a dislocation to form unless the shell consists of islands. Nucleation via surface loops must occur on planes tilted with respect to the interface such as the one depicted.

In both ZB and WZ heterowires, the dislocations that could be responsible for radial strain relaxation most efficiently are pure edge dislocations, line directions, **u** =[001] parallel to the growth, with tangential slip vectors (thicker dark lines in Fig. 11). In the ZB wires, such dislocations are known from planar studies of InAs growth on GaAs (110).[21] However, it is not clear from this previous study whether they formed via island coalescence, climb, or a Lomer-type reaction of two dislocations that glide on complementary planes.[24] A reaction mechanism is depicted in Fig. 11(a) requiring glide on higher energy {100} planes. In the WZ case, pure edge dislocations in nanowires have been observed[16] by viewing along the growth direction in cross-sections. In this case, the InAs core was hexagonally faceted with six $\{10\underline{1}0\}$ sidewall surfaces, Fig. 11(b). Pure edge dislocations with $\mathbf{b} = (a/6)\langle 11\underline{2}0\rangle$ were observed with spacing

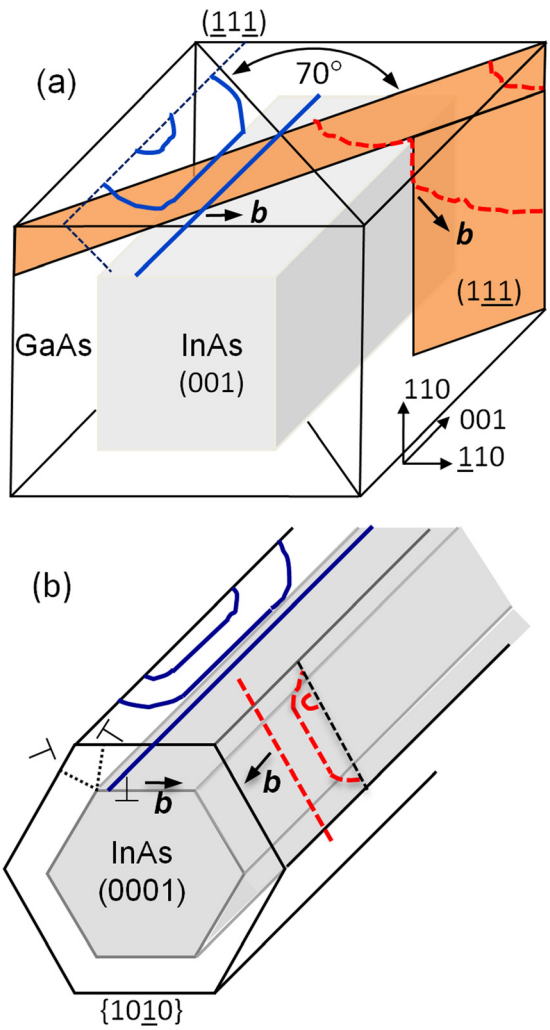

FIG. 11. (Color online) Schematic diagrams of feasible dislocations showing possible glide planes (shaded) for radial (dark lines) and axial (dotted lines) relaxation in (a) ZB and (b) WZ core–shell nanowires. In (a) a dislocation (dotted line) shown nucleating as a loop in the top right corner expands to the interfaces via glide on a $\{1\underline{1}1\}$ plane relaxing axial strain on the right sidewall (perpendicular component of **b**) and generating tilt and twist on the top facet with no strain relaxation. The pure edge dislocations (dark lines) relax radial strain forming perhaps via the reaction of two dislocations on complementary glide planes one is depicted. These could nucleate as loops at the surfaces (one set diagrammed) and then glide to the {110} interface but necessarily on more energetic planes (e.g., {100}) compared to $\{1\underline{1}1\}$.

consistent with the percentage radial strain relaxation measured from diffraction patterns. These dislocations could have formed directly by glide on $\{10\underline{1}0\}$ interface planes if the edge of the shell (e.g., islands) is available, by climb processes, or again by the reaction of two complementary perfect dislocations, edge components $\mathbf{b} = (\sqrt{3}a/2)\ \langle 10\underline{1}0\rangle$ depicted in Fig. 11(b). Similar to $\langle 1\underline{1}0\rangle$ Lomer dislocations in ZB systems,[24] these dislocations could nucleate at the surface then glide on two $\{11\underline{2}0\}$ planes inclined 30° to the interface.

Molecular statics calculations were used to understand better why radial relaxation is faster than axial. Calculations of the elastic strains for a Si–Ge[001] nanowire with a square 5 nm Ge core and a 2.5 nm Si shell oriented with (110) sides were scaled to determine the strains for an InAs–GaAs nanowire based on the relative lattice parameters and elastic constants. Ignoring end effects, the axial strains, ε_{zz}, were found to be uniform throughout both the core and shell with a compressive ε_{zz} of -4.0% in the InAs core and a tensile ε_{zz} of 3.1% in the GaAs shell. Normal strains, ε_{xx} and ε_{yy}, were greatest at the center of each interface. Parallel to the interface the strain was 4.5% in the shell, whereas normal to the interface, the compressive strain was 4.0% in both the core and shell. The in-plane normal strains decreased by 20% at the interface corners, whereas the shear strain, ε_{xy}, was 0.0 at the center of each interface, but increased dramatically at the corners as shown in Fig. 12.

Figure 12 plots the calculated ε_{xy} as a function of in-plane x–y position in the core and in the surrounding shell. The maximum magnitude of ε_{xy} is 7.9% at the interface corners, which is significantly higher than the normal strains. The strain energy density, calculated from the potential energy (stress × strain), is given to first order by $C_{11}\varepsilon_{xx}^2 + C_{11}\varepsilon_{yy}^2 + C_{11}\varepsilon_{zz}^2 + C_{44}\varepsilon_{xy}^2$, where the C_{11} and C_{44} are mechanical stiffness constants for each semiconductor. (For GaAs, $C_{11} = 119$ GPa, and $C_{44} = 59.6$ GPa, whereas for InAs, $C_{11} = 83.4$ GPa, and $C_{44} = 39.5$ GPa.) The total strain energy is found by integrating the strain energy density over a volume, which is proportional to the Burger's vector of the

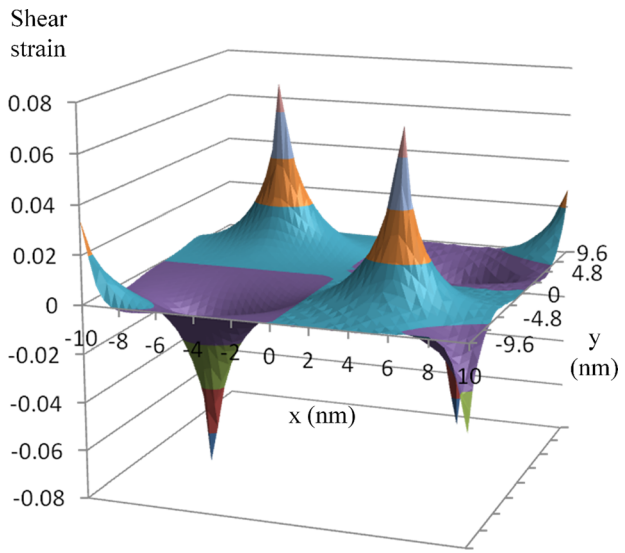

FIG. 12. (Color online) Shear strain ε_{xy} in a square InAs core (5 nm) surrounded by a GaAs shell (2.5 nm).

dislocation that forms. Due to the much higher ε_{xy} at the corners, the strain energy density is 45% higher there compared to at the center of each interface, but the volume where strain energy is relieved is the same.

The controlling factor for dislocation nucleation is the strain energy relieved by the dislocation, which will vary with the orientation of the dislocation. For nucleation of a dislocation that would reduce radial strain, the largest driving force is from the combination of the large ε_{xy} (7.9%) and the in-plane ε_{xx} (3.6%) at the corner of the interface. On the other hand, for reducing the axial strain, the driving force is only the uniform ε_{zz} in the shell (3.1%) and in the core (4.0%). The strain energy from axial strain is less than the strain energy from the normal strains at the corner. Therefore, when the additional contribution from shear strains is considered, the first dislocation nucleation would clearly be one that relieves radial strain in agreement with the experimental results.

V. CONCLUSIONS

The growth of InAs–GaAs (001) core–shell nanowires by molecular beam epitaxy (MBE) using Au nanoparticle catalysts has been investigated. The core InAs wires had either a square (ZB) or hexagonal (WZ) shape. A pronounced anisotropic growth rate of the GaAs shell for both zinc blende (ZB) and wurtzite (WZ) phase InAs core wires was observed. As the surface diffusivities of Ga and In atoms under the growth conditions used was greater than the wire length (at least 3 μm) we attribute the observed asymmetries to shadowing of the As flux. This resulted in the development of asymmetric strain relaxation, stacking faults and rotation that caused an overall curvature of the wires. Strain relaxation was observed via the formation of dislocations for GaAs shell thicknesses greater than 2 nm. Dislocations around the core that relax axial strain likely occurred via glide on {111} planes (ZB) along with generation of tilt on a perpendicular facet. In WZ nanowires the pure edge dislocations observed must have formed via climb or dislocation reactions unless island growth allowed glide on {1010} facet planes. The mechanism of formation of dislocations that relax radial strain was likely by glide and reaction on {11$\underline{2}$0} planes (WZ) or {100} planes (ZB). Relaxation was greater in radial compared to axial nanowire directions consistent with molecular statics calculations that predict a large shear stress at the interface corners.

ACKNOWLEDGMENTS

We thank the Canadian Institute for Photonics Innovation, the Natural Science and Engineering Research Council, and the Ontario Centres of Excellence for funding support.

[1]A. G. Cullis, A. J. Pidduck, and M. T. Emeny, J. Cryst. Growth **158**, 15 (1996).
[2]D. J. Eaglesham and M. Cerrullo, Phys. Rev. Lett. **64**, 1943 (1990).
[3]E. A. Fitzgerald, Mater. Sci. Rep. **7**, 87 (1991).
[4]M. Y. Gutkin, I. A. Ovid'ko, and A. G. Sheinerman, J. Phys. Condens. Matter **12**, 5391 (2000); I. A. Ovid'ko and A. G. Sheinerman, Philos. Mag. **84**, 2103 (2004); Adv. Phys. **55**, 627 (2006).
[5]G. Kastner and U. Gosele, Philos. Mag. **84**, 3803 (2004).
[6]E. Ertekin, P. A. Greaney, D. C. Chrzan, and T. D. Sands, J. Appl. Phys. **97**, 114325 (2005).
[7]F. Glas, Phys. Rev. B **74**, 121302 (R) (2006).
[8]S. Raychaudhuri and E. T. Yu, J. Appl. Phys. **99**, 114308 (2006); J. Vac. Sci. Technol. B **24**, 2053 (2006).
[9]T. E. Trammell, X. Zhang, Y. Li, L.-Q. Chen, and E. C. Dickey, J. Cryst. Growth **310**, 3084 (2008).
[10]K. L. Kavanagh, Semicond. Sci. Technol. **25**, 024006 (2010).
[11]K. L. Kavanagh, M. A. Capano, L. W. Hobbs, J. C. Barbour, P. M. J. Maree, W. Schaff, J. W. Mayer, D. Pettit, J. M Woodall, J. A. Stroscio, and R. M. Feenstra, J. Appl. Phys. **64**, 4843 (1988).
[12]M. A. Verheijen, R. E. Algra, M. T. Borgstrom, G. Immink, E. Soury, W. J. P. van Erickevort, E. Vlieg, and E. P. A. M. Bakkers, Nano Lett. **7**, 3051 (2007).
[13]V. Schmidt, P. C. McIntyre, and U. Gosele, Phys. Rev. B **77**, 235302 (2008); I. A. Goldthorpe, A. F. Marshall, and P. C. McIntyre, Nano Lett. **8**, 4081 (2008); Y. Liang, W. Nix, P. Griffin, and J. D. Plummer, J. Appl. Phys. **97**, 043519 (2005).
[14]S. Dayeh (private communication, 2011).
[15]M. Paladugu, J. Zou, Y.-N. Guo, X. Zhang, Y. Kim, H. J. Joyce, Q. Gao, H. H. Tan, and C. Jagadish, Appl. Phys. Lett. **93**, 101911 (2008); M. Paladugu, J. Zou, Y. N. Guo, X. Zhang, H. J. Joyce, Q. Gao, H. H. Tan, C. Jagadish, and Y. Kim, Nanoscale Res. Lett. **4**, 846 (2009).
[16]R. Popovitz-Biro, A. Kretinin, P. Von Huth, and H. Shtrikman, Cryst. Growth Des. **11**, 3858 (2011); H. Shtrikman, R. Popovitz-Biro, A. V. Kretinin, and P. Kacman, IEEE J. Sel. Top. Quantum Electron. **17**, 922 (2011).
[17]K. L. Kavanagh, J. Salfi, I. Savelyev, M. Blumin, and H. E. Ruda, Appl. Phys. Lett. **98**, 152103 (2011).
[18]S. Adachi, J. Appl. Phys. **53**, 8775 (1982); J. Appl. Phys. **58**, R1 (1985).
[19]M. I. McMahon and R. J. Nelmes, Phys. Rev. Lett. **95**, 215505 (2005).
[20]K. Tahahashi and K. Morizumi, Jpn. J. Appl. Phys. **5**, 657 (1966).
[21]J. G. Belk, D. W. Pashley, B. A. Joyce, and T. S. Jones, Phys. Rev. B **58**, 16294 (1998).
[22]Z. H. Wu, J. Q. Liu, X. Mei, D. Kim, M. Blumin, K. L. Kavanagh, and H. E. Ruda, Appl. Phys. Lett. **83**, 3368 (2003).
[23]A. Sasaki, J. Cryst. Growth **160**, 26 (1996).
[24]W. M. Lomer, Philos. Mag. **42**, 1327 (1951); E. P. Kvam, D. M. Maher, and C. J. Humpreys, J. Mater. Res. **5**, 1900 (1990); K. H. Chang, P. K. Bhattacharya, and R. Gibala, J. Appl. Phys. **66**, 2993 (1989).